Analytical model for optimizing the parameters of an external passive *Q*-switch in a fiber laser

J. Y. Huang, H. C. Liang, K. W. Su, and Y. F. Chen*

Department of Electrophysics, National Chiao Tung University, 1001 Ta Hsueh Road, Hsinchu 300, Taiwan

*Corresponding author: yfchen@cc.nctu.edu.tw

Received 26 October 2007; revised 21 March 2008; accepted 26 March 2008;
posted 26 March 2008 (Doc. ID 88437); published 28 April 2008

An analytical model is developed for optimizing two key parameters of an external passive *Q*-switch in a fiber laser from the criterion of the minimum average mode area inside the saturable absorber. One parameter is the optimum focal position that is analytically derived to be a function of the thickness and initial transmission of the saturable absorber. The other parameter is the optimum magnification of the reimaging optics that is analytically derived to be in terms of the numerical aperture and core radius of the laser fiber as well as the thickness and initial transmission of the saturable absorber. To demonstrate the utilization of the present model, an experiment on the subject of the passively *Q*-switched fiber laser is performed and optimized. © 2008 Optical Society of America

OCIS codes: 140.3540, 140.3510, 140.3615, 140.3430.

1. Introduction

The dominance of excellent beam quality, high efficiency, compactness and reliability has enabled diode-pumped rare-earth-doped double-clad fiber lasers to be very important light sources [1,2]. In recent years, high-peak-power *Q*-switched fiber lasers have attracted a great deal of attention because they are practically useful in numerous applications, such as range finding, remote sensing, industrial processing, and medicine [3–6]. Among various *Q*-switching methods, the passive *Q*-switching technique by means of saturable absorbers is particularly interesting from both a fundamental and a technological point of view. Up to now, Cr^{4+}-doped [7], Sm-doped [8], and Tm^{3+}–Yb^{3+} codoped [9] fibers have been developed as fiber saturable absorbers in fiber laser systems in the range of 1.0–1.1 μm.

Alternatively, the passive *Q*-switching of a fiber laser at 1.0–1.1 μm can be achieved by use of a Cr^{4+}-doped crystal [10–13] or a semiconductor material [14] as an external saturable absorber. The extended cavity consists of a reimaging optics to couple the laser mode into the saturable absorber [15]. In most cases, the average mode area inside the saturable absorber, A_s, significantly affects the output pulse energy and efficiency [16]. Therefore, it is important to develop a design model for optimizing the average mode area inside the saturable absorber.

Here we briefly describe the significance of A_s for the passive *Q*-switching operation and then derive A_s as an analytical function of the focal position of the reimaging mode, the numerical aperture and core size of the laser fiber, and the initial transmission and thickness of the saturable absorber. The analytical function enables us to obtain an explicit expression for the optimum focal position of the reimaging laser mode. Under the condition of minimum A_s, the optimum magnification of the reimaging optics is exactly derived in terms of the physical parameters of the laser fiber and the saturable absorber. The present model provides a straightforward procedure to determine the optimum reimaging magnification for an external passive *Q*-switch in a fiber laser. A practical example of an end-pumped Yb-doped fiber laser with a Cr^{4+}:YAG crystal as a saturable absorber is considered to illustrate the utilization of the present model.

2. Background

The coupled rate equations often used to model passively *Q*-switched lasers are generally based on the

0003-6935/08/132297-06$15.00/0

approximation of the uniform pumping of the gain medium, the intracavity optical intensity as axially uniform, and the complete recovery of the saturable absorber [17–19]. Including the focusing effect, the coupled equations for a four-level saturable absorber are given by [16,20]

$$\frac{\mathrm{d}\phi}{\mathrm{d}t} = \frac{\phi}{t_r}\left[2\sigma n l - 2\sigma_{\mathrm{gs}} n_{\mathrm{gs}} l_s - 2\sigma_{\mathrm{es}} n_{\mathrm{es}} l_s - \left(\ln\left(\frac{1}{R}\right) + L\right)\right], \tag{1}$$

$$\frac{\mathrm{d}n}{\mathrm{d}t} = -\gamma c \sigma \phi n, \tag{2}$$

$$\frac{\mathrm{d}n_{\mathrm{gs}}}{\mathrm{d}t} = -\frac{A}{A_s} c \sigma_{\mathrm{gs}} \phi n_{\mathrm{gs}}, \tag{3}$$

$$n_{\mathrm{gs}} + n_{\mathrm{es}} = n_{\mathrm{so}}, \tag{4}$$

where ϕ is the intracavity photon density with respect to the cross-sectional area of the laser beam in the gain medium, n is the population density of the gain medium, l_s is the length of the saturable absorber, A/A_s is the ratio of the average area in the gain medium and in the saturable absorber, n_{so} is the total population density of the saturable absorber, n_{gs} and n_{es} are the instantaneous population densities in the ground and excited states of the saturable absorber, respectively, σ_{gs} and σ_{es} are the ground-state absorption and excited-state absorption cross sections of the saturable absorber, respectively, R is the reflectivity of the output mirror, L is the round-trip dissipative optical losses, γ is the inversion reduction factor ($\gamma = 1$ and $\gamma = 2$ correspond to, respectively, four-level and three-level systems; see Ref. [17]), and $t_r = 2l'/c$ is the round-trip transit time of light in the cavity optical length l', where c is the speed of light. Note that although the approximation of uniform population inversion and photon density is not rigorously accurate, it has been confirmed to provide an excellent design guideline for solid-state lasers [16–18]. The experimental results shown in Section 5 validate the uniform approximation to be also applicable in fiber lasers.

Dividing Eq. (3) by Eq. (2) yields a separable first-order ordinary differential equation:

$$\frac{\mathrm{d}n_{\mathrm{gs}}}{\mathrm{d}n} = \frac{A}{A_s}\frac{1}{\gamma}\frac{\sigma_{\mathrm{gs}}}{\sigma}\frac{n_{\mathrm{gs}}}{n}. \tag{5}$$

Equation (5) can be solved to obtain

$$n_{\mathrm{gs}} = n_{\mathrm{so}}\left(\frac{n}{n_i}\right)^{\alpha}, \tag{6}$$

where n_i is the initial threshold value of the population inversion density in the gain medium at the start of Q-switching and the quantity α is given by

$$\alpha = \frac{1}{\gamma}\frac{\sigma_{\mathrm{gs}}}{\sigma}\frac{A}{A_s}. \tag{7}$$

We denote the quantity α to be the bleaching rate parameter (BRP) because its value determines the bleaching rate after the population inversion density reaches the initial threshold value.

With the coupled rate of Eqs. (1)–(4), the expression for the output pulse energy of the passively Q-switched laser has been derived to be given by [16,19]

$$E = \frac{h\upsilon A}{2\sigma\gamma}\ln\left(\frac{1}{R}\right)x, \tag{8}$$

where $h\upsilon$ is the laser photon energy, R is the reflectivity of the output mirror, and the parameter x represents the extraction efficiency of the energy stored in the gain medium through the lasing process. In terms of the BRP, the equation for the parameter x is given by

$$1 - e^{-x} - x + \frac{\left(1 - \sigma_{\mathrm{es}}/\sigma_{\mathrm{gs}}\right)\ln\left(1/T_o^2\right)}{\ln\left(1/T_o^2\right) + \ln\left(1/R\right) + L} \times \left(x - \frac{1 - e^{-\alpha x}}{\alpha}\right) = 0. \tag{9}$$

Note that in the calculation of the pulse energy with Eq. (8) the effect of cavity losses is included in the process of solving Eq. (9) with the parameter L. Furthermore, the nonlinear effects are not included in the present model because of the property of large mode areas of the fiber lasers studied here.

Equation (6) manifests that the larger the BRP, the faster the saturable absorber is bleached. As a consequence, the larger the BRP, the higher is the output efficiency of a passively Q-switching laser [16–19]. As indicated in Eq. (7), the BRP is proportional to the effective ratio A/A_s for a given gain medium and a given saturable absorber. Therefore, the optimization of the effective ratio A/A_s is essentially critical for developing an efficient passively Q-switched laser. For a given fiber laser, the maximization of the effective ratio A/A_s is directly related to the minimum A_s, as illustrated in Fig. 1. Since the minimum A_s is governed by the reimaging magnification M_a of the extended cavity, it is of practical usefulness to derive the optimum magnification in terms of the physical parameters of the laser fiber and the saturable absorber.

It is worthwhile to mention that the use of an external passive Q-switch and a high reflector is usually sufficient to completely prevent the CW lasing between the fiber end facets because the threshold is considerably reduced by the external feedback. The detailed discussion will be given in Section 5.

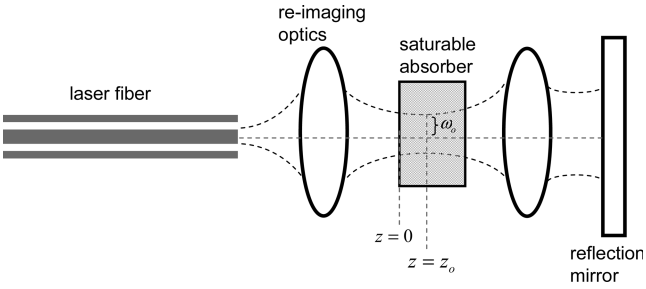

Fig. 1. Schematic illustration of the external cavity in a passively Q-switched fiber laser. ω_o is the beam waist of the laser mode; z_o is the position of the beam waist.

3. Optimization of Reimaging Magnification

The laser mode size in the saturable absorber is generally given by [21]

$$\omega_s(z) = \omega_o\sqrt{1 + [C(z - z_o)]^2}, \tag{10}$$

with

$$C = \frac{M^2\lambda}{\pi n_r \omega_o^2}, \tag{11}$$

where ω_o is the beam waist of the laser mode, z_o is the position of the beam waist, λ is the laser wavelength, M^2 is the beam-quality factor, n_r is the refractive index of the saturable absorber, and the point $z = 0$ is set at the incident surface of the saturable absorber. For a given core radius r_c, the beam waist in the saturable absorber is directly related to the reimaging magnification M_a by

$$\omega_o = M_a r_c. \tag{12}$$

With the brightness theorem, the beam-quality factor M^2 can be given by

$$M^2 = (NA \cdot r_c)(\pi/\lambda), \tag{13}$$

where NA is the numerical aperture of the laser fiber. Substituting Eqs. (12) and (13) into Eq. (11), the factor C can be expressed as

$$C = \frac{NA}{n_r M_a^{\,2} r_c}. \tag{14}$$

To take the round-trip effect into account, the average mode area in the saturable absorber, A_s, can be properly in terms of the mean square of the average mode size as

$$A_s = \pi\langle\omega_s^2\rangle \tag{15}$$

with

$$\langle\omega_s^2\rangle = \frac{\int_0^{l_a} \omega_s^2(z)[e^{-n_{so}\sigma_{gs}z} + e^{-n_{so}\sigma_{gs}(2l_a - z)}]\mathrm{d}z}{\int_0^{l_a}[e^{-n_{so}\sigma_{gs}z} + e^{-n_{so}\sigma_{gs}(2l_a - z)}]\mathrm{d}z}, \tag{16}$$

where l_a is the thickness of the saturable absorber and the weighting function $e^{-n_{so}\sigma_{gs}z}$ comes from the absorption effect. For the single-pass approximation, the effective beam area factor can be expressed as

$$\langle\omega_s^2\rangle = \frac{\int_0^{l_a} \omega_s^2(z)e^{-n_{so}\sigma_{gs}z}\mathrm{d}z}{\int_0^{l_a} e^{-n_{so}\sigma_{gs}z}\mathrm{d}z}. \tag{17}$$

Figure 2 shows a comparison for the calculated results $\langle\omega_s^2\rangle$ obtained with Eqs. (16) and (17) for a typical case with the parameters of $NA = 0.04$, $r_c = 12.5\,\mu$m, $n_r = 1.82$, $T_o = 0.4$, and $l_a = 2$ mm. It can be seen that the optimum focal position is shifted by approximately 0.2 mm when the round-trip effect is taken into account. Therefore, the influence of the round-trip effect on the effective beam area can be clearly found to be insignificant. Since Eq. (17) for the single-pass approximation leads the derivation to be more concise, it is used for optimizing the effective beam area. On the other hand, the standing-wave effect is omitted because the multilongitudinal mode operation of long fibers reduces this effect.

Substituting (10) into (17), the integration can be exactly carried out and the average mode area is expressed as

$$A_s = \pi\omega_o^2 C^2\left\{z_o^2 - 2z_o l_a\left[\frac{1}{\ln(1/T_o)} - \frac{T_o}{1 - T_o}\right] + \left[\frac{1}{C^2} + \frac{2l_a^2}{(\ln(1/T_o))^2} - l_a^2\left(\frac{T_o}{1 - T_o}\right)\left(1 + \frac{2}{\ln(1/T_o)}\right)\right]\right\}, \tag{18}$$

where $T_o = e^{-n_{so}\sigma_{gs}l_a}$ represents the initial transmission of the saturable absorber. Note that the expression of Eq. (18) is in term of the initial transmission T_o instead of $n_{so}\sigma_{gs}$ because T_o is a macroscopic property of the saturable absorber and can be definitely measured.

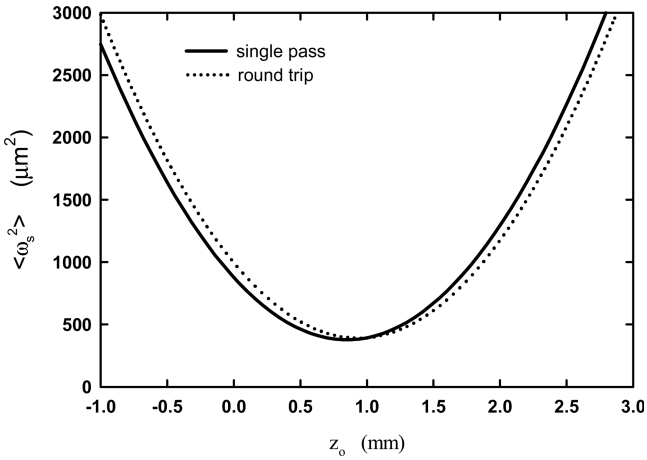

Fig. 2. A comparison for the calculated results $\langle\omega_s^2\rangle$ obtained with Eqs. (16) and (17) for a typical case with the parameters of $NA = 0.04$, $r_c = 12.5\,\mu$m, $n_r = 1.82$, $T_o = 0.4$, and $l_a = 2$ mm.

Figure 3 shows a calculated example with Eq. (18) and the parameters of $NA = 0.04$, $r_c = 12.5\,\mu$m, $n_r = 1.82$, and $l_a = 2$ mm to demonstrate the dependence of the average mode area on the focal position for several T_o values. It can be seen that there is an optimum focal position for minimizing the average mode area. The optimum focal position z_{opt} for the minimum mode area can be analytically determined by partially differentiating Eq. (18) with respect to z_o and setting the resulting equation equal to zero:

$$\left.\frac{\partial A_s}{\partial z_o}\right|_{z_o=z_{\text{opt}}} = 2\pi\omega_o^2 C^2 \times \left\{ z_{\text{opt}} - l_a\left[\frac{1}{\ln(1/T_o)} - \frac{T_o}{1-T_o}\right]\right\} = 0. \tag{19}$$

Equation (19) leads to the z_{opt} to be given by

$$z_{\text{opt}} = l_a\left[\frac{1}{\ln(1/T_o)} - \frac{T_o}{1-T_o}\right]. \tag{20}$$

Equation (20) indicates that the optimum focal position depends only on l_a and T_o, i.e., the properties of the saturable absorber. Substituting Eqs. (12), (14), and (20) into Eq. (18), the average mode area at the optimum focal position is then given by

$$A_s = \pi\left\{ {M_a}^2 r_c^2 + \frac{(NA)^2 l_a^2}{n_r^2 {M_a}^2}\left[\frac{1}{(\ln(1/T_o))^2} - \frac{T_o}{(1-T_o)^2}\right]\right\}. \tag{21}$$

The optimum magnification, M_{opt}, for minimizing the mode area can be analytically determined by partially differentiating Eq. (21) with respect to M_a and setting the resulting equation equal to zero:

$$\left.\frac{\partial A_s}{\partial M_a}\right|_{M_a=M_{\text{opt}}} = \pi\left\{ 2M_{\text{opt}} r_c^2 - \frac{2(NA)^2 l_a^2}{n_r^2 M_{\text{opt}}^3} \times \left[\frac{1}{(\ln(1/T_o))^2} - \frac{T_o}{(1-T_o)^2}\right]\right\} = 0. \tag{22}$$

Consequently, the M_{opt} is given by

$$M_{\text{opt}} = \left\{\frac{(NA)^2 l_a^2}{n_r^2 r_c^2}\left[\frac{1}{(\ln(1/T_o))^2} - \frac{T_o}{(1-T_o)^2}\right]\right\}^{1/4}. \tag{23}$$

Equation (23) indicates that the optimum reimaging magnification M_{opt} can be straightforwardly determined with the numerical aperture and core radius of the laser fiber as well as the thickness and initial transmission of the saturable absorber. Figure 4 depicts a calculated example with Eq. (22) and the parameters of $NA = 0.04$, $r_c = 12.5\,\mu$m, $n_r = 1.82$, and $T_o = 0.5$ to reveal the dependence of the average mode area on the magnification M_a for several l_a values. The dashed line in Fig. 4 shows the minimum average mode areas corresponding to the optimum magnification M_{opt}.

4. Experimental Results

To illustrate the utility of the present model, a Yb-doped fiber laser with a Cr^{4+}:YAG crystal as a saturable absorber is considered. Figure 5 shows the plot of the experimental setup that consists of a 1.5 m long fiber with a core diameter of 25 μm and a numerical aperture of 0.04. The fiber end facets were cut to be normal incident for the free-running operation. The pump source was a 13 W 976 nm fiber-coupled laser diode with a core diameter of 400 μm and a numerical aperture of 0.22. A focusing lens with 25 mm focal length and 92% coupling efficiency was used to reimage the pump beam into the fiber through a dichroic mirror with high transmission (>90%) at 976 nm and high reflectivity (>99.8%) at 1075 nm. The pump spot radius was approximately 200 μm.

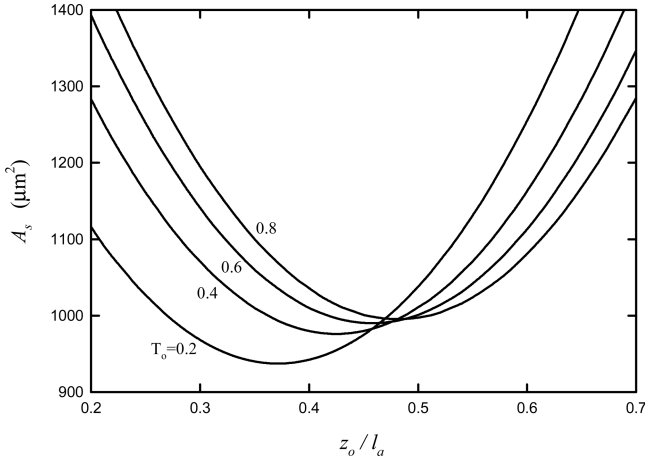

Fig. 3. Dependence of the average mode area on the focal position for several T_o values; the results are calculated with Eq. (18) and the parameters of $NA = 0.04$, $r_c = 12.5\,\mu$m, $n_r = 1.82$, and $l_a = 2$ mm.

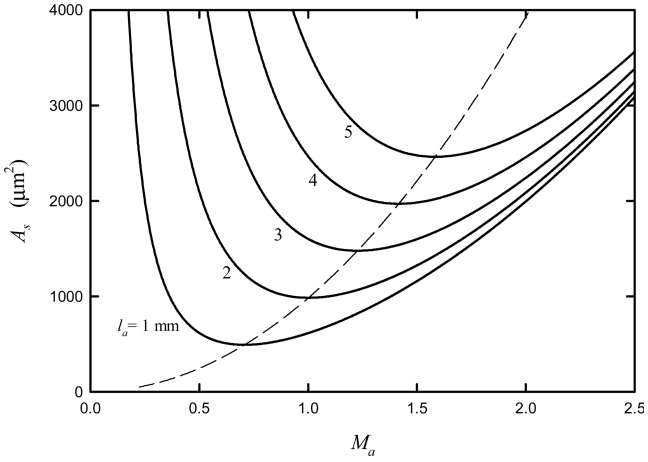

Fig. 4. Dependence of the average mode area on the magnification for several l_a values; the results are calculated with Eq. (22) and the parameters of $NA = 0.04$, $r_c = 12.5\,\mu$m, $n_r = 1.82$, and $T_o = 0.5$.

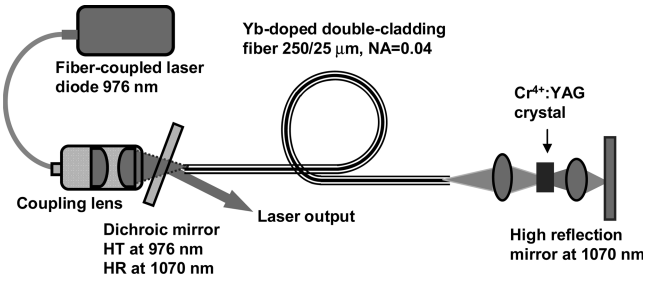

Fig. 5. Schematic setup of a diode-pumped passively Q-switched Yb-doped double-clad fiber laser. HR: high reflection; HT: high transmission.

The Cr^{4+}:YAG crystal has a thickness of 1.57 mm with 40% initial transmission at 1075 nm. Both sides of the Cr^{4+}:YAG crystal were coated for antireflection at 1075 nm ($R < 0.2\%$). The saturable absorber was wrapped with indium foil and mounted in a copper block without active cooling.

Substitution of the experimental parameters of $NA = 0.04$, $r_c = 12.5\,\mu$m, $n_r = 1.82$, $T_o = 0.4$, and $l_a = 1.57$ mm into Eq. (22) yields $M_{\text{opt}} = 0.88$. With the available optics, we setup an extended cavity to obtain a reimaging magnification of $M_a = 0.9$ that nearly achieves the optimum value of $M_{\text{opt}} = 0.88$. A translation stage was used to adjust the longitudinal position of the Cr^{4+}:YAG crystal for investigating the influence of the focal position on the average mode area as well as the output performance.

Figure 6 shows the experimental results for the dependence of the output pulse energy on the focal position at an incident pump power of 10 W. The theoretical calculations based on Eqs. (8) and (9) and the parameters of $\sigma = 2.4 \times 10^{-21}\,\text{cm}^2$ [22], $\sigma_{\text{gs}} = 8.7 \times 10^{-19}\,\text{cm}^2$ [23], $\sigma_{\text{es}} = 2.2 \times 10^{-19}\,\text{cm}^2$ [23], $R = 0.04$, and $L = 0.04$ are also shown in Fig. 6 for comparison. It can be seen that the output energy is significantly influenced by the focal position and the optimum focal position agrees very well with the theoretical analysis of $z_{\text{opt}} = 0.7$–0.9 mm.

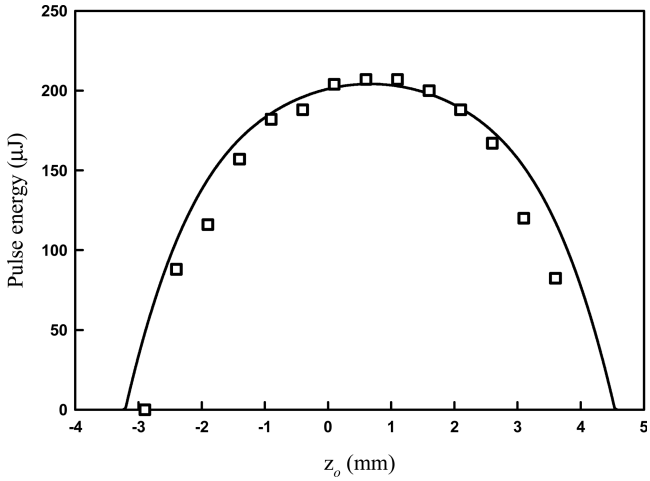

Fig. 6. Experimental and theoretical results for the output pulse energy as a function of the focal position. Symbols are experimental data. Solid line is calculated results using Eqs. (8) and (9).

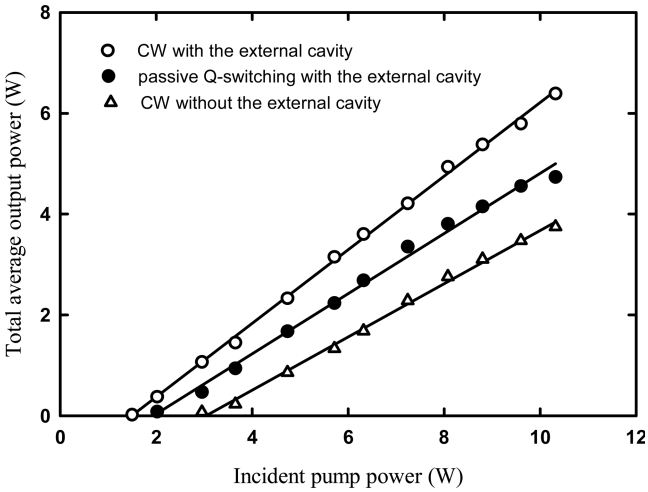

Fig. 7. Average output powers versus the incident pump power for CW lasing between facets, CW lasing with the external high-reflection cavity, and passive Q-switching operation with the external high-reflection cavity and the saturable absorber at the optimum focal position.

Although most of the fiber lasers can get CW lasing between facets without the external high-reflection cavity, the threshold of the fiber laser with an extended high-reflection cavity is considerably lower than that of the fiber laser without external feedback. Experimental results reveal that the threshold of the passive Q-switched fiber laser with an extended cavity is also usually lower than that of CW free-running operation between facets, as shown in Fig. 7. Since the extended cavity dominates the lasing, the couple-cavity effect arising from facets is insignificant in the performance of the passive Q-switching operation. Figure 8 shows the pulse repetition rate and the pulse energy versus the incident pump power at the optimum focal position. The pulse repetition rate initially increases with pump power, and is approximately up to 22 kHz at an incident pump power of 10 W. Like typically passively Q-switched lasers, the pulse energies weakly depend on the pump power and their values are found to be approximately 210 μJ. The pulse width is found to be in the range of 60–70 ns, as shown in the inset of Fig. 8.

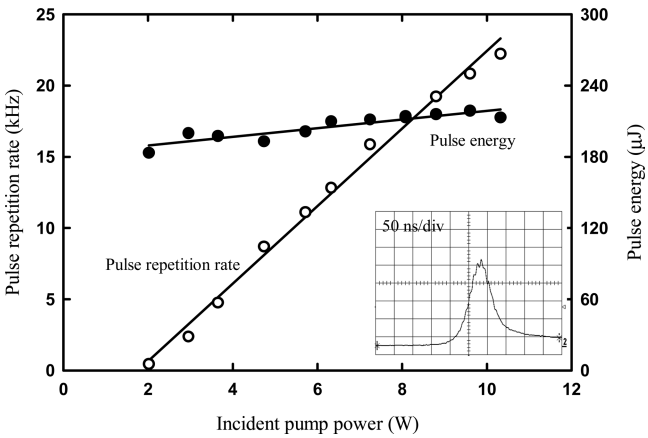

Fig. 8. Pulse repetition rate and pulse energy versus the incident pump power at the optimum focal position.

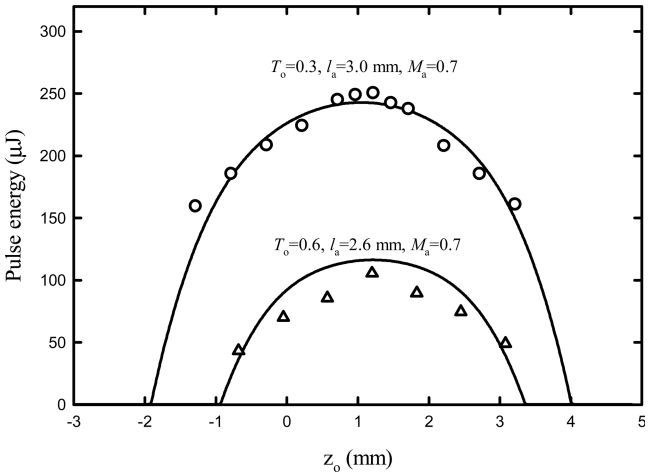

Fig. 9. Experimental and theoretical results for the dependence of the output pulse energy on the focal position at an incident pump power of 10 W. Symbols are experimental data. Solid line is calculated results using Eqs. (8) and (9).

To validate the developed models, two more experiments were performed with other saturable absorbers ($T_o = 0.3, l_a = 3.0$ mm and $T_o = 0.6, l_a = 2.6$ mm) and a reimaging magnification of $M_a = 0.7$. Figure 9 shows the experimental results for the dependence of the output pulse energy on the focal position at an incident pump power of 10 W. The good agreement between experimental results and theoretical predictions confirms the validity of our physical analysis.

5. Conclusion

We have developed an analytical model for the optimization of the extended cavity with a saturable absorber in a passively Q-switched fiber laser. From the criterion of the minimum average mode area inside the saturable absorber, the optimum focal position was derived to be an analytical function of the thickness and initial transmission of the saturable absorber. With the expression of the optimum focal position, the optimum magnification of the reimaging optics was exactly derived to be a compact close form in terms of the physical properties of the laser fiber as well as the saturable absorber. The present model provides a straightforward procedure to determine the key parameters for optimizing passively Q-switched fiber lasers. Finally, an experiment on the subject of the passively Q-switched fiber laser has been performed to validate the present model and to manifest the utilization.

References

1. L. Zenteno, "High-power double-clad fiber lasers," J. Lightwave Technol. **11**, 1435–1446 (1993).
2. M. J. F. Digonnet, *Rare-Earth-Doped Fiber Lasers and Amplifiers*, 2nd ed. (Marcel Dekker, 2001).
3. Z. J. Chen, A. B. Grudinin, J. Porta, and J. D. Minelly, "Enhanced Q-switching in double-clad fiber lasers," Opt. Lett. **23**, 454–456 (1998).
4. J. A. Alvarez-Chavez, H. L. Offerhaus, J. Nilson, P. W. Turner, W. A. Clarkson, and D. J. Richardson, "High-energy high-power ytterbium-doped Q-switched fiber laser," Opt. Lett. **25**, 37–39 (2000).
5. Y. X. Fan, F. Y. Lu, S. L. Hu, K. C. Lu, H. J. Wang, X. Y. Dong, J. L. He, and H. T. Wang, "Tunable high-peak-power, high-energy hybrid Q-switched double-clad fiber laser," Opt. Lett. **29**, 724–726 (2004).
6. B. N. Upadhyaya, U. Chakravarty, A. Kuruvilla, K. Thyagarajan, M. R. Shenoy, and S. M. Oak, "Mechanisms of generation of multi-peak and mode-locked resembling pulses in Q-switched Yb-doped fiber lasers," Opt. Express **15**, 11576–11588 (2007).
7. T. Tordella, H. Djellout, B. Dussardier, A. Saïssy, and G. Monnom, "High repetition rate passively Q-switched Nd^{3+}:Cr^{4+} all-fibre laser," Electron. Lett. **39**, 1307–1308 (2003).
8. A. Fotiadi, A. Kurkov, and I. Razdobreev, "All-fiber passively Q-switched ytterbium laser," in *CLEO/Europe-EQEC 2005*, Technical Digest, CJ 2–3 (IEEE, 2005).
9. P. Adel, M. Auerbach, C. Fallnich, S. Unger, H.-R. Müller, and J. Kirchhof, "Passive Q-switching by Tm^{3+} co-doping of a Yb^{3+}-fiber laser," Opt. Express **11**, 2730–2735 (2003).
10. M. Laroche, A. M. Chardon, J. Nilsson, D. P. Shepherd, W. A. Clarkson, S. Girard, and R. Moncorgé, "Compact diode-pumped passively Q-switched tunable Er-Yb double-clad fiber laser," Opt. Lett. **27**, 1980–1982 (2002).
11. V. N. Philippov, A. V. Kiryanov, and S. Unger, "Advanced configuration of erbium fiber passively Q-switched laser with Co^{2+}:ZnSe crystal as saturable absorber," IEEE Photonics Technol. Lett. **16**, 57–59 (2004).
12. F. Z. Qamar and T. A. King, "Passive Q-switching of the Tm-silica fiber laser near 2 μm by Cr^{2+}:ZnSe saturable absorber crystal," Opt. Commun. **248**, 501–505 (2005).
13. M. Laroche, H. Gilles, S. Girard, N. Passilly, and K. Aït-Ameur, "Nanosecond pulse generation in a passively Q-switched Yb-doped fiber laser by Cr^{4+}:YAG saturable absorber," IEEE Photon. Technol. Lett. **18**, 764–766 (2006).
14. R. Paschotta, R. Häring, E. Gini, H. Melchior, U. Keller, H. L. Offerhaus, and D. J. Richardson, "Passively Q-switched 0.1 mJ fiber laser system at 1.53 μm," Opt. Lett. **24**, 388–390 (1999).
15. Y. Wang and C. Q. Xu, "Modeling and optimization of Q-switched double-clad fiber lasers," Appl. Opt. **45**, 2058–2071 (2006).
16. Y. F. Chen, Y. P. Lan, and H. L. Chang, "Analytical model for design criteria of passively Q-switched lasers," IEEE J. Quantum Electron. **37**, 462–468 (2001).
17. J. J. Degnan, "Optimization of passively Q-switched lasers," IEEE J. Quantum Electron. **31**, 1890–1901 (1995).
18. G. Xiao and M. Bass, "A generalized model Q-switched lasers including excited state absorption in the saturable absorber," IEEE J. Quantum Electron. **33**, 41–44 (1997).
19. X. Zhang, S. Zhao, Q. Wang, Q. Zhang, L. Sun, and S. Zhang, "Optimization of Cr^{4+}-doped saturable-absorber Q-switched lasers," IEEE J. Quantum Electron. **33**, 2286–2294 (1997).
20. M. Hercher, "An analysis of saturable absorbers," Appl. Opt. **6**, 947–954 (1967).
21. A. E. Siegman, *Lasers* (University Science Books, 1986).
22. K. Lu and N. K. Dutta, "Spectroscopic properties of Yb-doped silica glass," J. Apl. Phys. **91**, 576–581 (2002).
23. Y. Shimony, Z, Burshtein, and Y. Kalisky, "Cr^{4+}:YAG as passive Q-switch and Brewster plate in a pulsed Nd:YAG laser," IEEE J. Quantum Electron. **31**, 1738–1741 (1995).